Inorg. Chem. **2000,** *39,* 4688−4695

Synthesis, Structural Characterization, and Monte Carlo Simulation of the Magnetic Properties of Two New Alternating Mn^{II} Azide 2-D Honeycombs. Study of the Ferromagnetic Ordered Phase below 20 K

Albert Escuer,[*,†] **Joan Cano,**[‡] **Mohamed A. S. Goher,**[§] **Yves Journaux,**[‡] **Francesc Lloret,**[||] **Franz A. Mautner,**[⊥] **and Ramon Vicente**[†]

Departament de Química Inorgànica, Universitat de Barcelona, Diagonal 647, E-08028 Barcelona, Spain,
Laboratoire de Chimie Inorganique, URA 420, CNRS, Université de Paris−Sud, F-91405 Orsay, France,
Chemistry Department, Faculty of Science, Alexandria University, P.O. Box 426 Ibrahimia,
Alexandria 21321, Egypt, Departament de Química Inorgànica, Universitat de València,
Doctor Moliner 50, 46100 Burjassot (València), Spain, and Institut für Physikalische und
Theoretische Chemie, Technische Universität Graz, A-8010 Graz, Austria

Received March 28, 2000

Reaction of Mn^{II} and pyridine derivatives such as 4-methylpyridine (4-Mepy) and 4-ethylpyridine (4-Etpy) led to the new two-dimensional systems *trans*-$[Mn(4\text{-}Mepy)_2(N_3)_2]_n$ (**1**) and *trans*-$[Mn(4\text{-}Etpy)_2(N_3)_2]_n$ (**2**). Compound **1** crystallizes in the triclinic system, $P\bar{1}$ group ($a = 9.269(2)$ Å, $b = 9.635(3)$ Å, $c = 18.860(4)$ Å, $Z = 4$), and compound **2** crystallizes in the monoclinic system, $P2_1/c$ group ($a = 14.416(3)$ Å, $b = 8.515(2)$ Å, $c = 15.728(4)$ Å, $Z = 4$). The two compounds show honeycomb structures based on dinuclear $Mn-(\mu\text{-}N_3)_2-Mn$ subunits linked to the four nearest-neighbor similar subunits by four end-to-end single azido bridges, but whereas the subunits of compound **1** show the end-to-end $Mn-(\mu_{1,3}\text{-}N_3)_2-Mn$ kind of bridges, compound **2** prefers the end-on $Mn-(\mu_{1,1}\text{-}N_3)_2-Mn$ fragment. Magnetically, compound **1** is an alternating 2-D system with two different antiferromagnetic interactions, whereas compound **2** corresponds to a two-dimensional ferro−antiferromagnetic system showing spin canting and permanent magnetization below 20 K. The coupling constant parameters $J_1 = -10.1$ cm^{-1}, $J_2 = -4.7$ cm^{-1}, and $g = 2.019$ for **1** and $J_1 = -5.3$ cm^{-1}, $J_2 = 2.9$ cm^{-1}, and $g = 2.016$ for **2** have been obtained from calculations using the Monte Carlo method based on the Metropolis algorithm.

Introduction

The exceptional ability of the azide anion to act as a bridge between two or more metallic centers in two main coordination modes such as the end-to-end (EE) and the end-on (EO), which act as a good mediator to transmit antiferromagnetic interactions (mainly EE bridges) or ferromagnetic interactions (mainly EO bridges), is the property that explains the large number of different magnetic systems based on the azide ligand reported in recent years.[1] Neutral manganese−azido complexes with general formula $[Mn(L)_2(N_3)_2]$, in which $(L)_2$ may be two monodentate pyridinic derivatives or one bidentate aromatic N-donor ligand, are one of the most versatile series of compounds from magnetic and structural points of view. Most compounds characterized to date are one-dimensional systems, and the appropriate combination of EE and EO bridges provides all the classical topologies. In fact, AF chains[2] (EE bridges), FM chains[2b,3] (EO bridges), or alternating AF/FM chains[4] (EE/EO bridges) have been characterized for several L ligands. Two topologies have been characterized to date for two-dimensional systems: square layers[5] with only EE single azido bridges (see Chart 1, left, for L = 4-acetylpyridine, methylisonicotinate, or diethylnicotinamide) and alternating AF/FM layers[6] with single EE/double EO azido bridges (see Chart 1, center, for L = 4-cyanopyridine, 3-acetylpyridine, ethylnicotinate, or ethylisonicotinate). Even a 3-D network was characterized for L = pyridine.[6b,7] Other high-dimensional manganese systems have been reported from the mixing of azido bridges with other N-donor polydentate bridging ligands.[3,8]

Development of high-dimensional coupled systems is a current research field, which may be of interest from theoretical or applied points of view. The above manganese−azido systems

---

* To whom correspondence should be addressed. E-mail: www.ub.es/inorgani/molmag.htm.

[†] Universitat de Barcelona.

[‡] Université de Paris−Sud.

[§] Alexandria University.

[||] Universitat de València.

[⊥] Technische Universität Graz.

(1) Ribas, J.; Escuer, A.; Monfort, M.; Vicente, R.; Cortés, R.; Lezama, L.; Rojo, T. *Coord. Chem. Rew.* **1999**, *193−195*, 1027.

(2) (a) Escuer, A.; Vicente, R.; Goher, M. A. S.; Mautner, F. A. *Inorg. Chem.* **1998**, *37*, 782. (b) Abu-Youssef, M. A. M.; Escuer, A.; Gatteschi, D.; Goher, M. A. S.; Mautner, F. A.; Vicente, R. *Inorg. Chem.* **1999**, *38*, 5716.

(3) Manson, J. L.; Arif, A. M.; Miller, J. S. *Chem. Commun.* **1999**, 1479.

(4) (a) Cortés, R.; Drillon, M.; Solans, X.; Lezama, L.; Rojo, T. *Inorg. Chem.* **1997**, *36*, 677. (b) Abu-Youssef, M.; Escuer, A.; Goher, M. A. S.; Mautner, F. A.; Vicente, R. *Eur. J. Inorg. Chem.* **1999**, 687. (c) Abu-Youssef, M.; Escuer, A.; Goher, M. A. S.; Mautner, F. A.; Vicente, R. *J. Chem. Soc., Dalton Trans.* **2000**, 413. (d) Abu-Youssef, M.; Escuer, A.; Goher, M. A. S.; Mautner, F. A.; Reiss, G.; Vicente, R. *Angew. Chem., Int. Ed. Engl.* **2000**, *39*, 1624.

(5) (a) Escuer, A.; Vicente, R.; Goher, M. A. S.; Mautner, F. A. *Inorg. Chem.* **1995**, *34*, 5707. (b) Escuer, A.; Vicente, R.; Goher, M. A. S.; Mautner, F. A. *J. Chem. Soc., Dalton Trans.* **1997**, 4431. (c) Goher, M. A. S.; Abu-Youssef, M.; Mautner, F. A.; Vicente, R.; Escuer, A. *Eur. J. Inorg. Chem.* **2000**, 1819.

(6) (a) Escuer, A.; Vicente, R.; Goher, M. A. S.; Mautner, F. A. *Inorg. Chem.* **1996**, *35*, 6386. (b) Escuer, A.; Vicente, R.; Mautner, F. A.; Goher, M. A. S. *Inorg. Chem.* **1997**, *36*, 3440. (c) Goher, M. A. S.; Al-Salem, N. A.; Mautner, F. A. *J. Coord. Chem.* **1998**, *44*, 119.

(7) Goher, M. A. S.; Mautner, F. A. *Croat. Chem. Acta* **1990**, *63*, 559.

10.1021/ic000335h CCC: $19.00 © 2000 American Chemical Society
Published on Web 09/21/2000

Chart 1

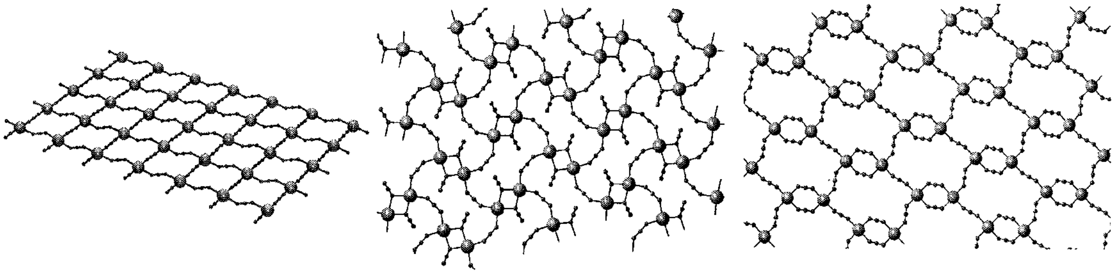

with complicated topologies affords good experimental examples to study new properties or check theories, such as the recent study of the EPR single-crystal spectra of one-dimensional systems with different magnetic interactions[2b] (AF, FM, or AF/FM systems) or the analysis of the magnetic properties of double chains with two *J* interactions or three-dimensional systems with three different superexchange pathways, corresponding to the general formula $C[Mn(N_3)_3]$ ($C = Cs^+$ or $N(Me)_4{}^+$), which have been analyzed by means of Monte Carlo simulations.[9]

Following our work in this field, we have focused our attention on the synthesis and structural characterization of two new two-dimensional compounds with general formula *trans*-$[Mn(L)_2(N_3)_2]_n$, in which L = 4-methylpyridine (4-Mepy), **1**, and 4-ethylpyridine (4-Etpy), **2**. It should be noted that compound **1** is the first example of a new metal−azido-layered topology (see Chart 1, right). Magnetically, compound **1** is an alternating system that shows two different antiferromagnetic interactions because of the regular arrangement of double and single EE azido bridges, whereas compound **2** is a ferro−antiferromagnetic alternating system derived from the regular arrangement of double EO and single EE azido bridges. Compound **2** exhibits global AF coupling, but at low temperature (below 20 K), it shows ferromagnetic long-range order and long-time magnetic relaxation.

To calculate the superexchange parameters for these complicated topologies, we have applied Monte Carlo simulations based on the Metropolis algorithm,[10] which seems to be the only method able to fit this kind of system to date in light of the results obtained with this kind of calculation on $S = {}^5/_2$ regular 1-D, 2-D, and 3-D extended systems and alternating chains for which alternative procedures exist.[11]

We present the synthesis, structural and magnetic properties, and the calculation of the coupling constant parameters for two different alternating honeycomb lattices.

Experimental Section

Spectral and Magnetic Measurements. Infrared spectra (4000−400 cm^{-1}) were recorded from KBr pellets on a Nicolet 520 FTIR spectrophotometer. Magnetic measurements were performed with a Quantum Design instrument with a superconducting quantum interference device (SQUID) detector working in the temperature range 300−2 K under external magnetic fields between 50 and 5000 G. Magnetization experiments were performed in the ±5 T range. Diamagnetic corrections were estimated from Pascal tables. EPR spectra were recorded at X-band frequency with a Bruker ES200 spectrometer equipped with an Oxford liquid-helium cryostat for variable temperature work.

Synthesis. $[Mn(4\text{-}Mepy)_2(N_3)_2]_n$ (**1**) was synthesized by mixing a water−methanolic solution (1:1, 30 mL) of manganese chloride tetrahydrate (0.59 g, 3 mmol) and 1.00 g (ca. 11 mmol) of 4-methylpyridine dissolved in 20 mL of methanol followed by dropwise addition of a concentrated aqueous solution of sodium azide (0.65 g, 10 mmol). To the resulting yellow-brown mixture, a few drops of L-ascorbic acid in methanol were added to keep it colorless and to prevent oxidation. The clear solution was left to stand in the dark for several days. Yellowish-green crystals suitable for X-ray determination were formed of complex **1** with a yield of ca. 60%. Anal. Calcd for $MnC_{12}H_{14}N_8$: C, 44.32; H, 4.34; N, 34.45; Mn, 16.89. Found: C, 44.2; H, 4.5; N, 34.6; Mn, 16.7. The IR spectra of **1** show the bands attributable to the 4-methylpyridine ligand at normal frequencies. In addition, complex **1** exhibits three bands centered around 2048 (vs), 2090 (vs), and 2126 (vs) cm^{-1}, which corresponds to the asymmetric azide vibration, and one band at 1332 cm^{-1}, which was assigned to the symmetric azide vibration ($\nu_s(N_3)$).

$[Mn(4\text{-}Etpy)_2(N_3)_2]_n$ (**2**) was prepared in the same way as compound **1** but using the following quantities of the starting reagents: 1.00 g (4 mmol) of manganese nitrate tetrahydrate, 1.07 g (10 mmol) of 4-ethylpyridine, and 0.65 g (10 mmol) of sodium azide. The resulting solution was kept in the dark for about 2 weeks to yield large well-formed yellow crystals of compound **2**. Yield, ca. 65%. Anal. Calcd for $MnC_{14}H_{18}N_8$: C, 47.60; H, 5.14; N, 31.72; Mn, 15.55. Found: C, 47.7; H, 5.2; N, 31.4; Mn, 15.4. Complex **2** also shows three bands at 2055 (vs), 2076 (vs), and 2109 (vs) cm^{-1} but in contrast to **1** does not show absorption bands in the 1290−1370 cm^{-1} region.

Crystallographic Data Collection and Refinement of the Structures of $[Mn(4\text{-}Mepy)_2(N_3)_2]_n$ (1) and $[Mn(4\text{-}Etpy)_2(N_3)_2]_n$ (2)

The X-ray single-crystal data for both compounds were collected on a modified STOE four-circle diffractometer. Crystal sizes were 0.53 mm × 0.35 mm × 0.20 mm for **1** and 0.55 mm × 0.40 mm × 0.18 mm for **2**. The crystallographic data, conditions retained for the intensity data collection, and some features of the structure refinements are listed in Table 1. Graphite-monochromatized Mo Kα radiation ($\lambda = 0.710\,69$ Å) and the ω-scan technique was used to collect the data sets. The accurate unit-cell parameters were determined from automatic centering of 44 reflections ($9.2° < \theta < 11.5°$) for **1** and 81 reflections ($8.7° < \theta < 12.9°$) for **2** and refined by least-squares methods. A total of 5270 reflections (4835 independent reflections, $R_{int} = 0.0298$) were collected for **1** in the range $2.76° < \theta < 25.00°$ and 3912 reflections (3130 independent reflections, $R_{int} = 0.0338$) were collected for **2** in the range $2.80° < \theta < 26.00°$. The observed intensity decay of control reflections (1 1 3; 1 3 7) was 27% in the case of **1** and 33% for control reflections (0 1 3; 3 0 −8) in the case of **2**. Corrections were applied for Lorentz polarization effects, for intensity decay, and for absorption using the DIFABS[12] computer program (range of normalized transmission coefficients is 0.518−1.000 for **1**

---

(8) (a) Shen, H. Y.; Liao, D. Z.; Jiang, Z. H.; Yan, S. P.; Sun, B. W.; Wang, G. L.; Yao, X. K.; Wang, H. G. *Chem. Lett.* **1998**, 469. (b) De Munno, G.; Julve, M.; Viau, G.; Lloret, F.; Faus, J.; Viterbo, D. *Angew. Chem., Int. Ed. Engl.* **1996**, *35*, 1807. (c) Cortés, R.; Lezama, L.; Pizarro, J. L.; Arriortua, M. I.; Rojo, T. *Angew. Chem., Int. Ed. Engl.* **1996**, *35*, 1810. (d) Tang, L. F.; Zhang, L.; Li, L. C.; Cheng, P.; Wang, Z. H.; Wang, J. T. *Inorg. Chem.* **1999**, *38*, 6326.

(9) Goher, M. A. S.; Cano, J.; Journaux, Y.; Abu-Youssef, M. A. M.; Mautner, F. A.; Escuer, A.; Vicente, R. *Chem.−Eur. J.* **2000**, *6*, 778.

(10) Metropolis, N.; Rosenbluth, A. W.; Rosenbluth, M. N.; Teller, A. H.; Teller, E. *J. Chem. Phys.* **1953**, *21*, 1087.

(11) Cano, J.; Journaux, Y. *Mol. Cryst. Liq. Cryst.* **1999**, *335*, 1397.

Table 1. Crystal Data and Structure Refinement for $[Mn(4\text{-}Mepy)_2(N_3)_2]_n$ (**1**) and $[Mn(4\text{-}Etpy)_2(N_3)_2]_n$ (**2**)

	1	**2**
chem formula	$C_{12}H_{14}MnN_8$	$C_{14}H_{18}MnN_8$
fw	325.25	353.30
space group	$P\bar{1}$	$P2_1/c$
a, Å	9.269(2)	14.416(3)
b, Å	9.635(3)	8.515(2)
c, Å	18.860(4)	15.728(4)
α, deg	80.52(2)	90.00
β, deg	83.65(2)	117.06(2)
γ, deg	62.81(2)	90.00
V, Å^3	1476.5(6)	1719.3(7)
Z	4	4
temp, °C	22(2)	22(2)
λ (Mo Kα), Å	0.710 69	0.710 69
d_{calc}, g cm^{-3}	1.463	1.365
μ(Mo Kα), mm^{-1}	0.900	0.779
$^aR_1$	0.0519	0.0523
$^bwR^2$	0.1155	0.1143

^{a} $R_1(F_o) = \sum(F_o - F_c)/\sum F_o$. ^{b} $wR^2(F_o)^2 = \{\sum[w((F_o)^2 - (F_c)^2)^2]/\sum[w(F_o)^4]\}^{1/2}$.

and 0.492−1.000 for **2**). The structures were solved by direct methods using the SHELXS-86 computer program[13] and refined by full-matrix least-squares methods on F^2, using the SHELXL-93 computer program[14] incorporated in SHELXTL/PC, version 5.03, program package.[15] Some plots were prepared from PLATON computer program.[16] All non-hydrogen atoms were refined anisotropically. The hydrogen atoms were obtained from ΔF maps and subsequently located on calculated positions, and their isotropic displacement parameters were fixed with the equivalent U values of the parent C atoms. In the case of **2**, atoms C(14) and C(15) of the disordered ethyl group were assigned occupation factors 0.78 and 0.22, respectively. The final R indices were 0.0519 and 0.0523, respectively, for all observed reflections. Number of refined parameters was 383 (**1**) and 220 (**2**). Maximum and minimum peaks in the final difference Fourier syntheses were 0.338 and −0.247 e Å^{-3} (**1**) and 0.245 and −0.333 eÅ^{-3} (**2**). Significant bond parameters for **1** and **2** are given in Tables 2 and 3, respectively.

Table 2. Selected Bond Lengths (Å) and Angles (deg) for $[Mn(4\text{-}Mepy)_2(N_3)_2]_n$ (**1**)

Manganese Environment			
Mn(1)−N(1)	2.291(3)	Mn(2)−N(3)	2.304(3)
Mn(1)−N(2)	2.279(3)	Mn(2)−N(4)	2.270(3)
Mn(1)−N(11)	2.240(3)	Mn(2)−N(23)	2.204(4)
Mn(1)−N(13A)	2.257(4)	Mn(2)−N(33B)	2.177(4)
Mn(1)−N(21)	2.199(3)	Mn(2)−N(41)	2.263(3)
Mn(1)−N(31)	2.169(4)	Mn(2)−N(43C)	2.239(3)
N(1)−Mn(1)−N(2)	172.6(1)	N(3)−Mn(2)−N(4)	172.6(1)
N(1)−Mn(1)−N(11)	87.4(1)	N(3)−Mn(2)−N(23)	92.3(1)
N(1)−Mn(1)−N(13A)	87.2(1)	N(3)−Mn(2)−N(33B)	92.5(2)
N(1)−Mn(1)−N(21)	89.8(1)	N(3)−Mn(2)−N(41)	86.8(1)
N(1)−Mn(1)−N(31)	93.7(2)	N(3)−Mn(2)−N(43C)	87.3(1)
N(2)−Mn(1)−N(11)	89.8(1)	N(4)−Mn(2)−N(23)	90.3(1)
N(2)−Mn(1)−N(13A)	86.0(1)	N(4)−Mn(2)−N(33B)	94.4(2)
N(2)−Mn(1)−N(21)	92.8(1)	N(4)−Mn(2)−N(41)	86.3(1)
N(2)−Mn(1)−N(31)	93.2(2)	N(4)−Mn(2)−N(43C)	89.9(1)
N(11)−Mn(1)−N(13A)	89.8(1)	N(23)−Mn(2)−N(33B)	90.8(2)
N(11)−Mn(1)−N(21)	177.0(1)	N(23)−Mn(2)−N(41)	87.9(1)
N(11)−Mn(1)−N(31)	90.8(1)	N(23)−Mn(2)−N(43C)	178.2(1)
N(13A)−Mn(1)−N(21)	88.9(1)	N(33B)−Mn(2)−N(41)	178.5(1)
N(13A)−Mn(1)−N(31)	178.9(2)	N(33B)−Mn(2)−N(43C)	91.0(1)
N(21)−Mn(1)−N(31)	90.5(2)	N(41)−Mn(2)−N(43C)	90.3(1)
Mn(1)−N(11)−N(12)	119.7(3)	N(12)−N(13)−Mn(1A)	134.3(3)
Mn(1)−N(21)−N(22)	135.8(3)	N(22)−N(23)−Mn(2)	137.0(3)
Mn(1)−N(31)−N(32)	162.8(4)	N(32B)−N(33B)−Mn(2)	161.6(4)
Mn(2)−N(41)−N(42)	133.7(3)	N(42)−N(43)−Mn(2C)	122.6(3)
Azido Groups			
N(11)−N(12)	1.178(4)	N(12)−N(13)	1.167(4)
N(21)−N(22)	1.164(4)	N(22)−N(23)	1.157(4)
N(31)−N(32)	1.143(4)	N(32)−N(33)	1.139(4)
N(41)−N(42)	1.170(4)	N(42)−N(43)	1.177(4)
N(11)−N(12)−N(13)	178.1(4)	N(21)−N(22)−N(23)	179.4(4)
N(31)−N(32)−N(33)	179.1(5)	N(41)−N(42)−N(43)	177.9(4)

Table 3. Selected Bond Lengths (Å) and Angles (deg) for $[Mn(4\text{-}Etpy)_2(N_3)_2]_n$ (**2**)

Manganese Environment			
Mn(1)−N(1)	2.273(4)	Mn(1)−N(2)	2.278(4)
Mn(1)−N(11)	2.250(4)	Mn(1)−N(11A)	2.276(4)
Mn(1)−N(21)	2.197(4)	Mn(1)−N(23B)	2.206(4)
N(1)−Mn(1)−N(2)	173.8(1)	N(11)−Mn(1)−N(11A)	77.8(2)
N(1)−Mn(1)−N(11)	90.9(1)	N(11)−Mn(1)−N(21)	91.2(2)
N(1)−Mn(1)−N(11A)	91.2(1)	N(11)−Mn(1)−N(23B)	167.1(2)
N(1)−Mn(1)−N(21)	89.0(2)	N(11A)−Mn(1)−N(21)	169.0(2)
N(1)−Mn(1)−N(23B)	86.6(2)	N(11A)−Mn(1)−N(23B)	89.6(2)
N(2)−Mn(1)−N(11)	94.9(1)	N(21)−Mn(1)−N(23B)	101.4(2)
N(2)−Mn(1)−N(11A)	91.9(1)		
N(2)−Mn(1)−N(21)	88.9(2)		
N(2)−Mn(1)−N(23B)	88.1(2)		
Mn(1)−N(11)−N(12)	124.3(3)	N(12)−N(11)−Mn(1A)	123.0(3)
Mn(1)−N(21)−N(22)	150.3(4)	N(22)−N(23)−Mn(1C)	143.9(4)
Mn(1)−N(11)−Mn(1A)	102.2(2)		
Azido Groups			
N(11)−N(12)	1.179(5)	N(12)−N(13)	1.155(5)
N(21)−N(22)	1.155(5)	N(22)−N(23)	1.156(5)
N(11)−N(12)−N(13)	179.9(5)	N(21)−N(22)−N(23)	176.7(5)

$[Mn(4\text{-}Mepy)_2(N_3)_2]_n$ (1). An ORTEP scheme of **1** is shown in Figure 1. This compound may be properly described as manganese dimeric units linked by a double end-to-end azide bridge, which are connected to the four neighboring similar units by means of four single end-to-end azido bridges (Figure 2). Repetition of this basic unit affords a neutral two-dimensional layer. There are two nonequivalent Mn−$(N_3)_2$−Mn centrosymmetric subunits in these layers. Subunit A, defined by the Mn(1)/Mn(1A) environment, shows Mn(1)−N(11)−N(12) and Mn(1A)−N(13)−N(12) bond angles of 119.7(3)° and 134.3(3)°, whereas the subunit B, defined by the Mn(2)/Mn(2C) environment, shows Mn(2)−N(41)−N(42) and Mn(2C)−N(43)−N(42) bond angles of 133.7(3)° and 122.6(3)°, respectively. Mn−N bond lengths inside the rings are similar for Mn(1) and Mn(2), in the 2.239−2.263 Å range. In the two A and B groups the azido bridging ligands are parallel, but the manganese atom is displaced out of this plane, giving a chair distorted ring. The distortion of this ring, measured as δ or τ parameters,[2] is 29.9(2)° or 54.3(4)° for ring A and 26.4(2)° or 48.4(2)° for ring B, respectively. Manganese atoms are 0.793(1) Å (A unit) and 0.705(1) Å (B unit) out of the corresponding N azido mean planes. Subunit A is linked to two B subunits by a single azido bridge, showing Mn(1)−N(21)−N(22) and N(22)−N(23)−Mn(2) bond angles of 135.8(3)° and 137.0(3)° and a τ torsion angle of 179.3(5)°, and to two other A groups, also linked by a single bridge with Mn(1)−N(31)−N(32) and N(32B)−N(33B)−Mn(2) of 162.8(4)° and 161.6(4)°, respectively, and a τ torsion angle

---

(12) Walker, N.; Stuart, D. *Acta Crystallogr.* **1983**, *A39*, 158.

(13) Sheldrick, G. M. *SHELXS-86, Program for the Solution of Crystal Structure*; University of Göttingen: Göttingen, Germany, 1986.

(14) Sheldrick, G. M. *SHELXL-93, Program for the Refinement of Crystal Structure*; University of Göttingen: Göttingen, Germany, 1993.

(15) *SHELXTL 5.03 (PC version), Program library for the Solution and Molecular Graphics*; Siemens Analytical Instruments Division: Madison, WI, 1995.

(16) Spek, A. L. *PLUTON-92*; University of Utrecht: Utrecht, The Netherlands, 1992.

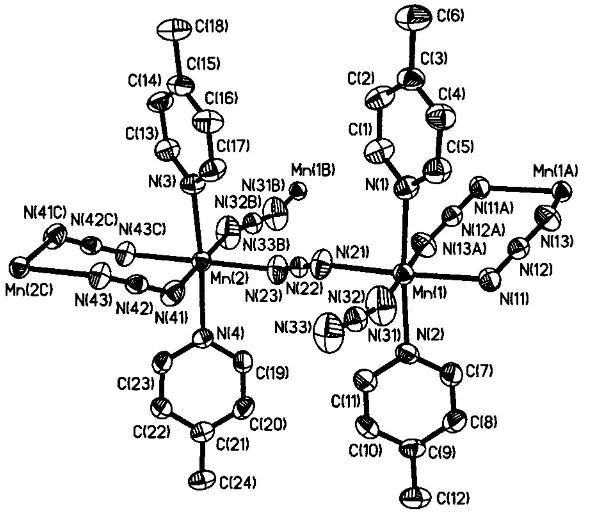

Figure 1. ORTEP drawing for $[Mn(4\text{-}Mepy)_2(N_3)_2]_n$ (**1**). Ellipsoids are at the 50% probability level.

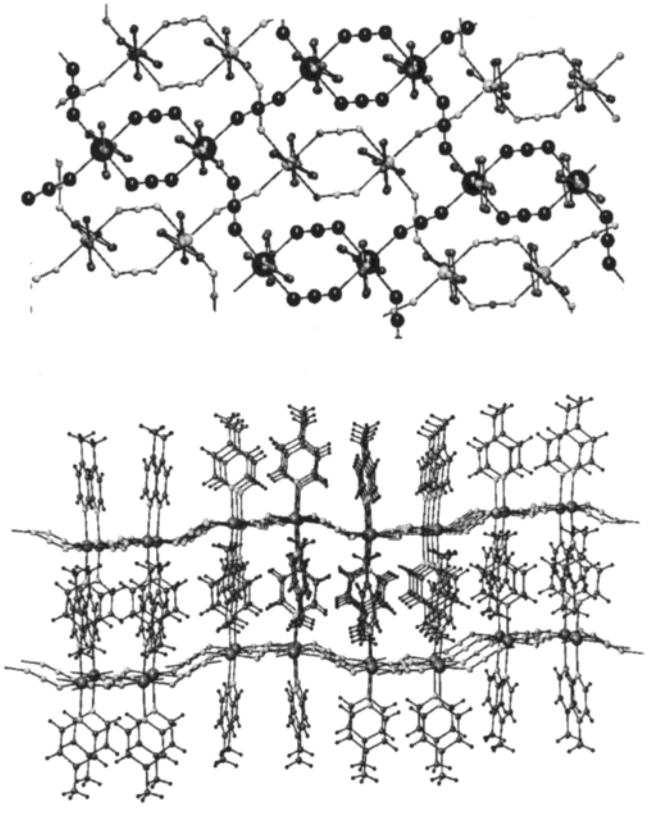

Figure 2. Packing view of $[Mn(4\text{-}Mepy)_2(N_3)_2]_n$ (**1**): (top) view close to the N(1)−Mn−N(2) axis, showing the arrangement of the layers (one as dark and greater balls and the next layer as smaller gray balls); (bottom) view along (0 1 0) direction, showing the relatively short interplane separation.

of 174.7(1)°. The intralayer Mn$\cdots$Mn distance is similar in A and B units; Mn(1)$\cdots$Mn(1A) is 5.335(2) Å and Mn(2)$\cdots$Mn(2C) is 5.374(2) Å and shorter than Mn(1)$\cdots$Mn(2), 6.290(2) Å, or Mn(1B)$\cdots$Mn(2), 6.556(2) Å, according to the respective Mn−N−N bond angles.

The minimum interlayer Mn$\cdots$Mn distance is 9.052 Å, and several Mn atoms are closer than 10 Å (Figure 2). This interlayer separation for **1** is significantly shorter than those found to date in other 2-D $[Mn(L)_2(N_3)_2]$ systems, for which typical interlayer distances are between 13 and 17 Å.[5,6] This short separation between consecutive planes is a consequence of several factors, such as the large size of the six Mn atoms rings (main axis, 13.678 Å × 9.635 Å), the planar arrangement of the layers derived from the low torsion angles through the single azido bridges, and the reduced size of the 4-methyl group. As is shown in Figure 2, each $Mn-(N_3)_2-Mn$ unit is placed at the center of the six Mn atoms ring of the next plane with the methyl groups in this large space. No $\pi-\pi$ interactions between the aromatic rings of the different planes are present in this case.

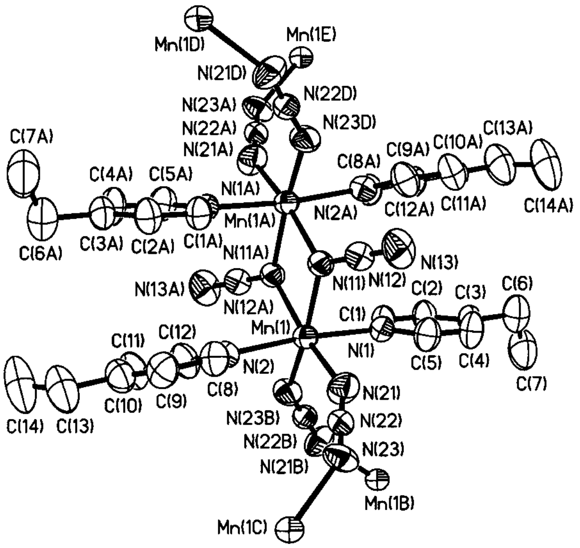

Figure 3. ORTEP drawing for $[Mn(4\text{-}Etpy)_2(N_3)_2]_n$ (**2**). Ellipsoids are at the 50% probability level.

$[Mn(4\text{-}Etpy)_2(N_3)_2]_n$ (2). The ORTEP plot of **2** is shown in Figure 3. In this case the manganese dimeric units are linked by one double end-on azide bridge. Each dimeric fragment is linked to the four neighboring equivalent units by means of four single end-to-end azido bridges. Repetition of this basic scheme affords, as in the 4-Mepy compound, a neutral two-dimensional layer (Figure 4). The four-membered Mn_2N_2 rings are strictly planar, showing a Mn(1)−N(11)−Mn(1A) bond angle of 102.2(2)° and a Mn(1)$\cdots$Mn(1A) distance of 3.523(1) Å. The single azido bridge shows the Mn(1)−N(21)−N(22) and the N(22)−N(23)−Mn(1C) bond angles of 150.3(4)° and 143.9(4)°, respectively, a τ dihedral angle of 91.8(6)°, and a larger Mn(1)$\cdots$Mn(1B) distance of 6.083(1) Å.

The minimum interlayer Mn$\cdots$Mn distance in this case is 13.274 Å, within the normal range found to date. In contrast to compound **1**, the reduced size of the six Mn atoms ring (12.209 Å × 8.515 Å), the large torsion angles through the single azido bridges, which determine an angle of 86.6(1)° between the equatorial coordination plane of neighboring manganese atoms, and the larger size of the 4-ethyl group allow the larger interlayer separation (Figure 4).

Magnetic Behavior

The room-temperature values of $\chi_M T$ of 3.42 cm^3 K mol^{-1} for compound **1** and 3.88 cm^3 K mol^{-1} for compound **2** are significantly lower than that expected for a magnetically isolated Mn(II) ion (4.375 cm^3 K mol^{-1} with $g = 2$). In both cases, $\chi_M T$ decreases on cooling and it vanishes when T approaches zero. The susceptibility curves (Figure 5) show maxima at 58 K (**1**) and 38 K (**2**). These features are characteristic of a dominant antiferromagnetic interaction for both compounds. The χ_M value of **1** tends to 1.7×10^{-2} cm^3 mol^{-1} when T tends to

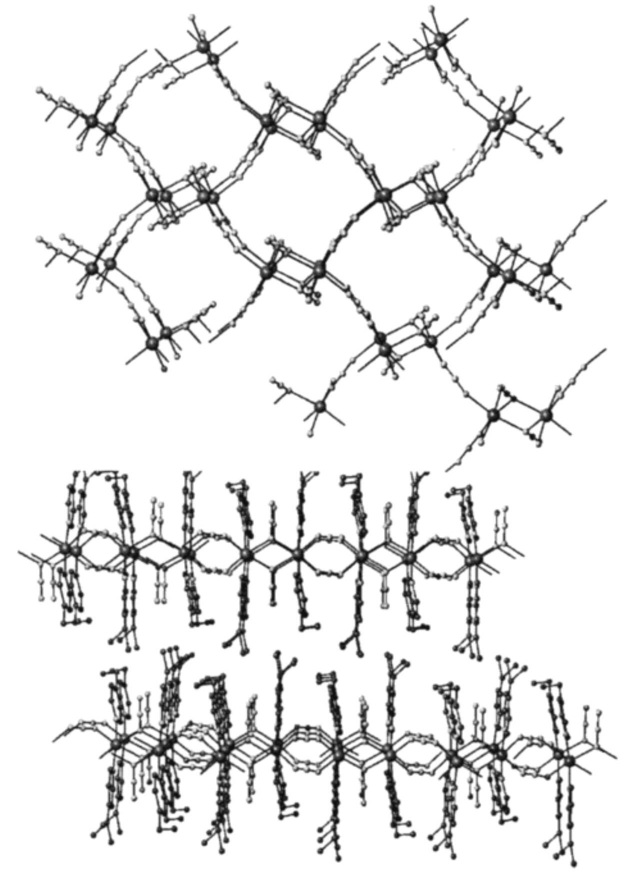

Figure 4. Packing view of $[Mn(4\text{-}Etpy)_2(N_3)_2]_n$ (**2**): (top) view along (1 0 0) direction showing the arrangement of the layers; (bottom) view along (0 1 0) direction showing the large interplane distance.

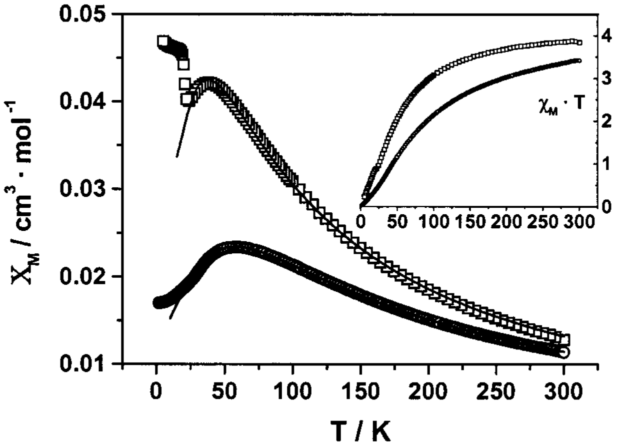

Figure 5. Plot of the molar susceptibility and χ_MT (inset) vs T for $[Mn(4\text{-}Mepy)_2(N_3)_2]_n$ (**1**), plotted as open circles, and for $[Mn(4\text{-}Etpy)_2(N_3)_2]_n$ (**2**), plotted as open squares. Solid lines correspond to the Monte Carlo procedure best fits.

zero, in close agreement with the value expected[17a] for the perpendicular component of the susceptibility in the case of an antiferromagnetic ordered lattice ($\chi_{per} \approx (^2/_3)\chi_{max}$, χ_{max} being ca 2.4×10^{-2} cm^3 mol^{-1}). In contrast, the magnetic behavior of **2** is much more complex. The susceptibility curve undergoes an abrupt increase below 23 K, and it reaches saturation very quickly ($\chi_M = 4.8 \times 10^{-2}$ cm^3 mol^{-1} at 2 K and under an applied field of 5000 G), as shown in Figure 5.

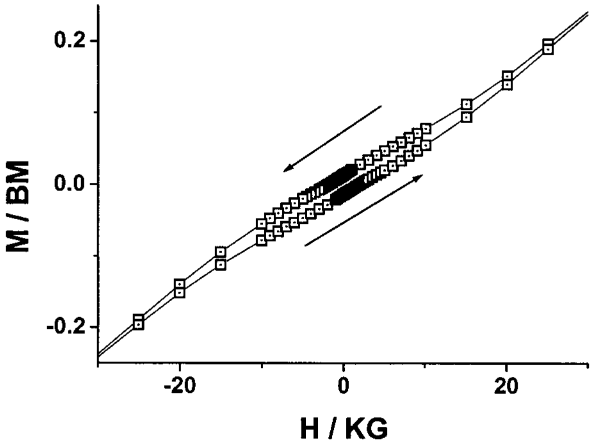

Figure 6. Magnetization measurement at 1.9 K for $[Mn(4\text{-}Etpy)_2(N_3)_2]_n$ (**2**), showing the hysteresis loop. The maximum field used in this measurement was ±5 T. Solid lines are a guide for the eye.

Magnetization measurements for **2**, performed in the ±5 T range, show a hysteresis loop (Figure 6). These series of magnetic phenomena in the low-temperature range will be widely discussed below.

EPR spectra for the two compounds show the expected coupling-narrowed isotropic signals centered at $g = 2.00$ in the 300−150 K range of temperature, with a peak-to-peak line width of 16 G for **1** and 55 G for **2**. Below this temperature ΔH_{pp} increases on cooling as a consequence of the dipolar interactions, reaching 500 G for **1** at 21 K. For **2** a complicated nonisotropic pattern of broad signals appears below 15 K, with three main bands centered at $g = 3.57$, 2.51, and 2.02.

Magnetic Behavior in the High-Temperature Region. Monte Carlo Simulation. The infinite number of possible configurations for extended systems prevents the exact calculation of the partition function and, consequently, the derivation of the thermodynamic properties (magnetic susceptibility, specific heats, etc.) for complicated topologies. To tackle the calculation of thermodynamic properties of infinite networks, physicists have developed approximate methods such as high-temperature expansion of the partition function,[17b] closed-chain computational procedure,[18] and a density matrix renormalization group approach (DMRG).[19,20] Nevertheless, all these approaches are either of limited application (DMRG) or difficult to implement (high-temperature expansion). Among all these approximate methods, Monte Carlo simulation seems to be the only one with a wide range of application. So, to analyze the magnetic properties of our $S = {}^5/_2$ systems, we used the Monte Carlo method based on the Metropolis algorithm[10] considering a classical spin Hamiltonian.

As described, **1** and **2** are honeycomb-layered compounds where the Mn(II) ions are bridged by azido ligands. These systems may be assumed as antiferromagnetically coupled (J_1) zigzag regular chains of manganese atoms bridged by EE single azido ligands, which interact through double azido bridges, EE for compound **1** with AF coupling or EO for compound **2** with FM coupling (J_2).

To study the magnetic properties of these Heisenberg alternating honeycomb lattices, we have considered the isotropic

---

[17] (a) De Jongh, L. J. In *Magnetic Properties of Layered Transition Metal Compounds*; de Jongh, L. J., Ed.; Kluwer Academic Publishers: Dordrecht, The Netherlands, 1990; Chapter 1. (b) Navarro, R. In *Magnetic Properties of Layered Transition Metal Compounds*; de Jongh, L. J., Ed.; Kluwer Academic Publishers: Dordrecht, The Netherlands, 1990; Chapter 3.

[18] Bonner, J. C.; Fischer, M. E. *Phys. Rev.* **1964**, *A135*, 640.

[19] White, S. R.; Noack, R. M. *Phys. Rev. Lett.* **1992**, *68*, 3487.

[20] White, S. R.; Huse, D. A. *Phys. Rev. B* **1993**, *48*, 3844.

exchange Hamiltonian written as

$$H = -J_1 \sum_{i=1,j=1} S_{i,j}S_{i,j+1} - J_2 \sum_{\substack{i=1\\ j=1\\ i+j=\text{odd}}} S_{i,j}S_{i+1,j}$$

where the index of S represents the site, J the exchange coupling constants that are restricted to the nearest neighbors, and S the classical spin operators. This approximation is justified for the manganese(II) ion because it exhibits a large spin ($S = {}^5/_2$).[21,22] To make a quantitative comparison, we have scaled the classical spin to a real quantum spin using the following scaling factor:

$$S_i \rightarrow \sqrt{S_i(S_i + 1)}$$

The Monte Carlo simulations were based on the Metropolis algorithm,[10] which generates a sampling of states following the Boltzmann distribution. The magnetic susceptibility, χ, is related to the fluctuations of the magnetization as

$$\chi = \frac{1}{kT}(\langle M^2\rangle - \langle M\rangle^2)$$

where $\langle M\rangle$ and $\langle M^2\rangle$ are the mean values of M and M^2 and where M is the magnetization.

The 2×10^5 Monte Carlo steps per site (MCS) were performed, and the first 2×10^4 were discarded as the initial transient stage. To avoid the freezing of the spin configuration, we used a low cooling rate according to $T_{i+1} = 0.95T_i$, where T represents the temperature.

To select the lattice size, we have performed simulations on models with several numbers of sites. Hence, we have first determined the minimum sample where no finite-size effects are observed within the studied reduced-temperature (T/J) range. Consequently, a 256 (16 × 16) sites sample was chosen for this study, which is 3 times larger than the minimum sample. To avoid any perturbation from the edge of the sample and to speed the convergence toward the infinite lattice limit, we considered periodic boundary conditions (PBC).[23]

So, we have considered the temperature range 300−18 K for **1** and 300−24 K for **2**. Good fits were obtained with the following set of parameters: $J_1 = -10.1$ cm^{-1}, $J_2 = -4.7$ cm^{-1}, and $g = 2.019$ for **1**; $J_1 = -5.3$ cm^{-1}, $J_2 = 2.9$ cm^{-1}, and $g = 2.016$ for **2**. The agreement factors R, defined as $\sum[(\chi_M)_{obsd} - (\chi_M)_{calcd}]^2/\sum[(\chi_M)_{obsd}]^2$, were equal to 3.0×10^{-5} for **1** and 5.6×10^{-5} for **2** (Figure 5). These results lie in the normal range of interactions previously reported for one-dimensional systems with double EE or EO azido bridges.[2−4]

We have performed spin topology maps without interlayer interaction at different temperatures for **2**. The results are shown in Chart 3. For clarity, only a 12 × 8 fragment from the 16 × 16 ferroantiferromagnetic honeycomb network used for the simulation is represented. It is well established that for 2D networks with isotropic interaction, there is no long-range order[24,25] and domains with opposite spin direction should appear in the map. But because of the small number of spins in our sample, it is not possible to reveal the formation of these domains, and this feature is reinforced by the periodic boundary conditions. Nevertheless, these maps show interesting features. At high temperature, all the possible spin orientations are equally probable and there is no correlation between neighboring spins. As the temperature is lowered, short-range ordering slowly appears and in the map at $T = 0.1$ K all the spin orientations are correlated with respect to the topology of the ferromagnetic interactions in one direction and to the antiferromagnetic interactions in the other.

Chart 2

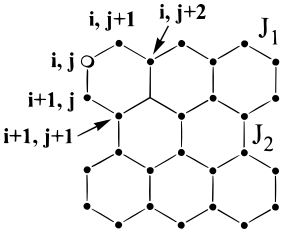

Chart 3

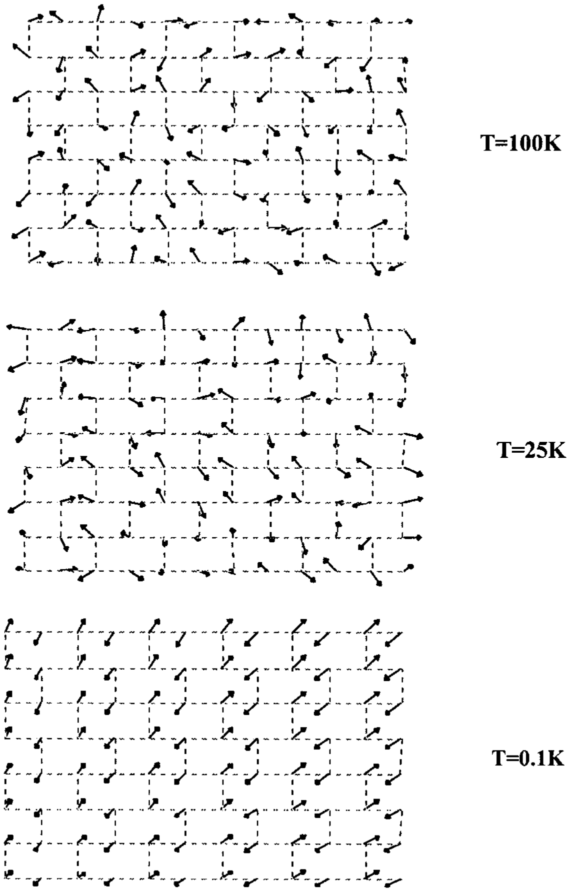

Magnetic Behavior in the Low-Temperature Region for Compound 2. As indicated above, whereas compound **1** shows the characteristic behavior of a two-dimensional Heisenberg antiferromagnet, compound **2** shows an abrupt increase of susceptibility below 23 K, which may suggest the occurrence of a spin-canting structure at $T < 23$ K and which deserves a more detailed study.

However, the susceptibility curve exhibits an additional maximum at 20 K for $H < 4000$ G. As is shown in Figure 7, this maximum is clearly defined as the magnetic field is decreased. This phenomenon is characteristic of a metamagnetic system with a critical magnetic field H_c of 4000 G. This metamagnetic behavior can also be observed in the magnetiza-

---

(21) Fischer, M. E. *Am. J. Phys.* **1964**, *32*, 343.

(22) Kahn, O. In *Molecular Magnetism*; VCH Publishers Inc.: New York, 1993.

(23) Binder, K.; Heermann, D. W. *Monte Carlo Simulation in Statistical Physics. An introduction*; Fulde, P., Ed.; Springer Series in Solid-State Sciences, 3rd ed.; Springer: Berlin, 1997.

(24) Mermin, N. D.; Wagner, H. *Phys. Rev. Lett.* **1966**, 1133.

(25) Kosterlitz, J. M.; Thouless, D. J. *J. Phys. C: Solid State Phys.* **1973**, 1181.

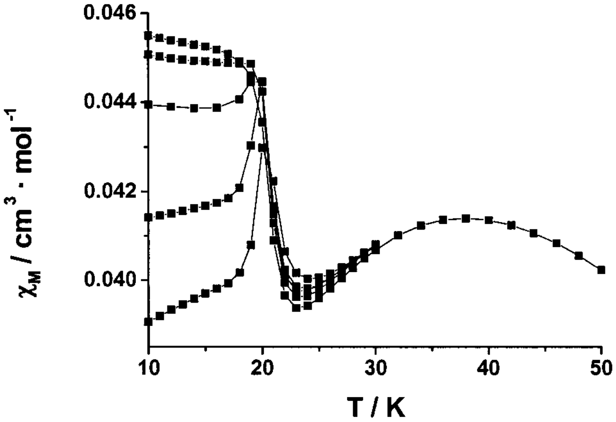

Figure 7. Plot of the molar susceptibility vs T for $[Mn(4\text{-}Etpy)_2(N_3)_2]_n$ (**2**), measured on cooling under external magnetic fields of 4500, 4000, 3500, 3000, and 2500 G (from top to bottom in the plot). Solid lines are a guide for the eye.

Chart 4

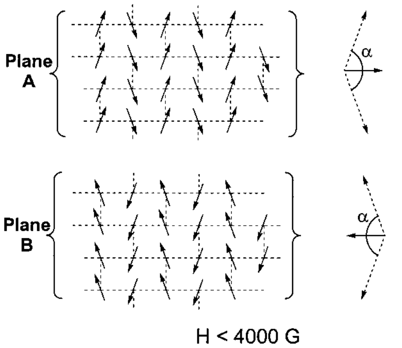

tion experiments as a function of the applied magnetic field at 1.9 K. The sample was cooled in the absence of a magnetic field and its magnetization, M, was measured by applying the magnetic field. For small applied fields (H < 4000 G), the magnetization increases linearly with the field and the slope increases for higher fields, but the values of M are far below that expected for a total alignment of spins ($M \approx 5\ \mu_B$). Even at 5 T (the highest field available to us), the value of the magnetization is less than 0.4 μ_B (8% of the total magnetization).

The magnetic behavior of **2** can be understood as follows. In the absence of magnetic anisotropy and/or antisymmetric exchange, the intrasheet isotropic magnetic interactions would orientate the local spin of the Mn(II) ions as indicated in Chart 3 (spin arrangement obtained by Monte Carlo simulation at 0.1 K). In this scheme, the local spins cancel each other, leading to a zero magnetic moment. Under these isotropic conditions, the susceptibility curve would exhibit the maximum at 39 K, vanishing at $T = 0$ K.

The sharp increase in susceptibility at T < 23 K suggests that the local spins adopt a spin-canting structure within the sheet, schematized in Charts 4 and 5, which would account for the abrupt increase in χ_M. In low magnetic fields (H < 4000 G), the intersheet antiferromagnetic interactions would cause the antiparallel spin arrangement of the adjacent sheets (A and B planes in Chart 4) and the subsequent cancellation of the magnetic moment of **2** (maximum of susceptibility at 20 K). However, stronger magnetic fields (H > 4000 G) provide enough energy to break the intersheet antiferromagnetic interactions, and a parallel spin arrangement of the adjacent sheets results (planes A and B in Chart 5). In this situation, **2** exhibits a nonzero magnetic moment, which accounts for the lack of the susceptibility maximum and the change of the slope in the magnetization curve.

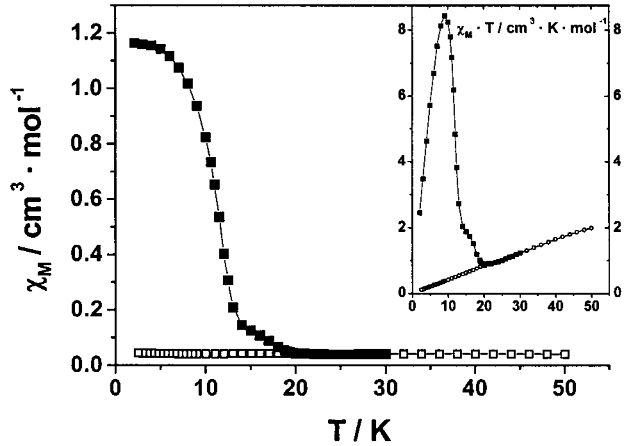

Figure 8. Plot of the molar susceptibility and $\chi_M T$ (inset) vs T for $[Mn(4\text{-}Etpy)_2(N_3)_2]_n$ (**2**), measured on cooling under a magnetic field of 50 G (open squares) and at increasing temperature at the same field, after 1 min at 2 K under 1 T (filled squares). Solid lines are a guide for the eye.

Chart 5

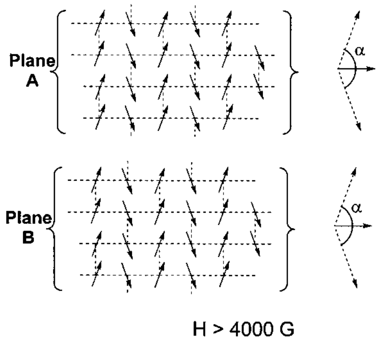

Curiously, despite the instability of the parallel spin alignment of the adjacent sheets (Chart 5) with respect to the antiparallel one (Chart 4) in the absence of a magnetic field (or H < 4000 G), this magnetic structure remains metastable at T < 20 K and $H = 0$. Thus, once **2** has been magnetized at 1.9 K under a strong magnetic field, it exhibits a remnant magnetization, Mr, of 0.0135 μ_B and a coercive field, Hc, of 1950 G (see hysteresis loop in Figure 6) when the applied field progressively decreases. The hysteresis loop is observed for T < 20, but the values of Mr and Hc decrease as T increases (Mr = 0.0125 μ_B and Hc = 1800 G at $T = 5$ K; Mr = 0.008 μ_B and Hc = 950 G at T 10 K).

To determine the temperature of magnetic ordering of the spin-canted structure, the sample was cooled to 2 K, then a magnetic field of +1 T was applied for 1 min, then the field was decreased to 50 G, and the magnetization of the metastable magnetic phase (Chart 5) was measured while the temperature was increased. The result is shown in Figure 8 in the form of χ_M and $\chi_M T$ (inset) versus T plots. For the sake of comparison, the corresponding curve of the antiferromagnetic phase (Chart 4) is shown. In this last case, the sample was cooled to 2 K and then a magnetic field of 50 G was applied and the magnetization was measured as a function of the temperature. At $T \approx 20$ K both curves collapse, indicating that the spin-canting phase only occurs for temperatures below 20 K.

Finally, the time dependence for the remnant magnetization of the metastable spin-canting structure (Chart 5) was studied. The sample was cooled from 30 K to a well-defined temperature

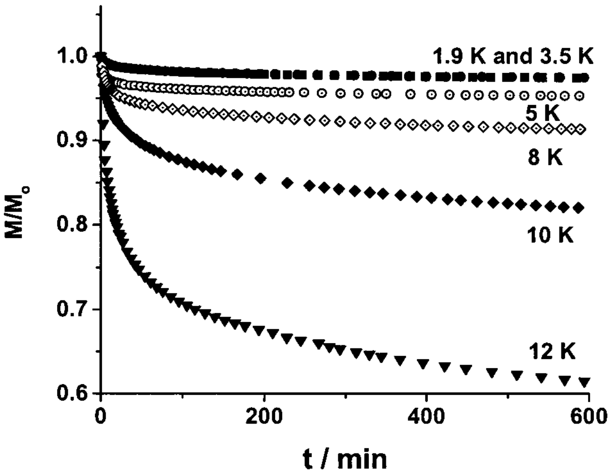

Figure 9. Plot of M/M_0 vs time at five different temperatures for $[Mn(4\text{-}Etpy)_2(N_3)_2]_n$ (**2**).

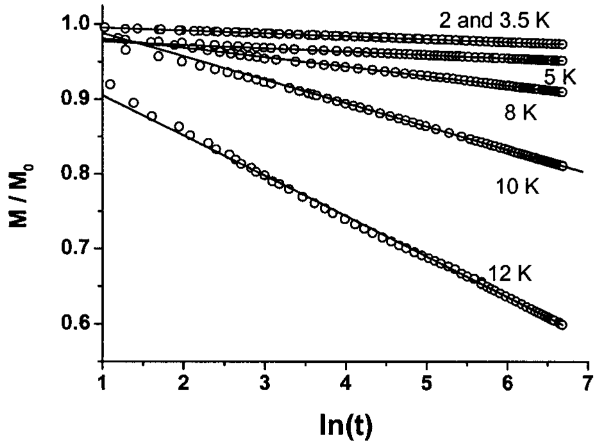

Figure 10. Plot showing the linear dependence of M/M_0 vs ln(t) at five different temperatures for $[Mn(4\text{-}Etpy)_2(N_3)_2]_n$ (**2**). Solid lines show the simulated dependence (see text).

(T < 20 K) in the presence of a field of 5 T. Then the field was rapidly removed. The time dependence of the magnetization was followed for about 15 h. The time interval between two consecutive $M(t)$ points was 2 min. The M/M_0 ratio versus time at different temperatures is shown in Figure 9. M is the magnetization and M_0 its asymptotic value, which is basically the same as the value of Mr obtained from the corresponding hysteresis loop.

All these curves show a pronounced long-time magnetic relaxation, and they exhibit logarithmic decay, as expected for a set of particles with different energy barriers. Figure 10 shows the linear dependence[26] of M/M_0 versus ln(t) expected from the equation

$$\frac{M}{M_0} = 1 - S(T)\ln\frac{t}{t_0}$$

Solid lines represent the fits to this expression. The value of the magnetic viscosity, $S(T)$, for each temperature is given by the slope of corresponding straight line (M/M_0 versus ln(t) plot in Figure 10). The $S(T)$ values obtained are $S(12\text{ K}) = 53.6 \times 10^{-3}$, $S(10\text{ K}) = 31.3 \times 10^{-3}$, $S(8\text{ K}) = 12.4 \times 10^{-3}$, $S(5\text{ K}) = 4.5 \times 10^{-3}$, $S(3.5\text{ K}) = 3.9 \times 10^{-3}$, and $S(2\text{ K}) = 3.9 \times 10^{-3}$ (Figure 11). The magnetic viscosity is proportional to the temperature and should increase linearly with T for a thermal relaxation.[26] However, the values of $S(T)$ in the 2−5 K range appear almost temperature-independent as is shown in Figure 11. The presence of this constant value suggests nonthermal relaxation at low temperature and the occurrence of quantum tunneling of the magnetization. However, the experimental $S(T)$ values at high temperature do not extrapolate to zero at $T = 0$, in disagreement with the theory. So, although this nonthermal relaxation could be ascribed to the occurrence of quantum tunneling of the magnetization, further experiments are needed to rule out any experimental artifact.

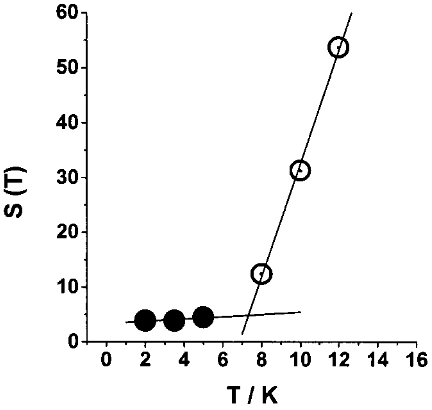

Figure 11. Plot of the magnetic viscosity $S(T)$ vs T for $[Mn(4\text{-}Etpy)_2(N_3)_2]_n$ (**2**), showing the different behavior between T < 5 K (filled circles) and T > 5 K (dot centered circles). Solid lines are a guide for the eye.

Conclusion

Two new two-dimensional alternating honeycomb Mn^{II} azido systems have been characterized from magnetic and structural points of view. Long-range order and long-time relaxation phenomena have been found for compound **2** at T < 20 K. Good agreement between numerical simulation and experiment is obtained, showing that the Monte Carlo method is a good tool to study $S = {}^5/_2$ alternating honeycomb lattices. Furthermore, this approach is easily applicable to other networks and interaction topologies, which opens wide perspectives in molecular magnetism.

Acknowledgment. A.E. and R.V. thank the CICYT (Grant PB96-163) for supporting this research. F.A.M. and M.A.M. A.-Y. thank Prof. C. Kratky and Dr. F. Belaj (University of Graz) for use of experimental equipment; and the Oesterreichische Nationalbank (Jubilaeumsfondsprojekt 6630) for financial support.

Supporting Information Available: Three X-ray cryatallographic files, in CIF format. This material is available free of charge via the Internet at http://pubs.acs.org.

IC000335H

---

[26] Tejada, J.; Zhang, X. X.; Chudnovsky, E. M. *Phys. Rev. B* **1993**, *47*, 14977.